Paleoceanography and Paleoclimatology

RESEARCH ARTICLE
10.1029/2021PA004375

Special Section:
DeepMIP in the Hothouse Earth: late Paleocene - early Eocene climates and their lessons for the future

Variations on a Pathway to an Early Eocene Climate

Matthew Henry[1] **and Geoffrey K. Vallis**[1]

[1]Department of Mathematics, University of Exeter, Exeter, UK

Key Points:

- We offer physically plausible mechanisms for the warm winter climates over land in the Eocene
- Model simulations verify the mechanisms, and suggest that no exotic additional physics is needed
- High CO_2 levels are essential, but various combinations of other parameters satisfy proxy data

Correspondence to:
M. Henry,
m.henry@exeter.ac.uk

Citation:
Henry, M., & Vallis, G. K. (2022). Variations on a pathway to an early Eocene climate. *Paleoceanography and Paleoclimatology*, *37*, e2021PA004375. https://doi.org/10.1029/2021PA004375

Received 25 OCT 2021
Accepted 26 JUL 2022

Abstract The climate of the early Eocene was characterized by much higher temperatures and a smaller equator-to-pole surface temperature gradient than today. Comprehensive climate models have been reasonably successful in simulating that climate in the annual average. However, good simulations of the seasonal variations, and in particular much warmer Arctic winters over land, have proven more difficult. Further, while increased greenhouse gases seems necessary to achieve an Eocene climate, it is unclear whether there is a unique combination of factors that leads to agreement with all available proxies. Here we use a very flexible General Circulation Model to examine the sensitivity of the modeled climate to differences in CO_2 concentration, land surface properties, ocean heat transport, and cloud extent and thickness. Even in the absence of ice or changes in cloudiness, increasing the CO_2 concentration leads to a polar-amplified surface temperature change because of increased water vapor levels combined with the lack of convection at high latitudes, with the nonlinear dependence of longwave radiation on temperature amplifying the increase in winter over land. Additional low clouds over Arctic land generally decrease summer temperatures and further increase winter temperatures (except at very high CO_2 levels). An increase in the land surface heat capacity, plausible given large changes in vegetation, also decreases the Arctic land seasonality. Thus, different combinations of factors—high CO_2 levels, changes in low-level clouds, and an increase in land surface heat capacity—can lead to a simulation within the proxy uncertainty range of the majority of proxy data.

Plain Language Summary During the early Eocene, some 50 million years ago, the Earth was approximately 13°C warmer and the equator-to-pole surface temperature difference was much smaller than it is today. We now have proxy data on the surface temperature at different latitudes and the seasonality of the surface temperature (for land at high-latitudes), the amount of carbon dioxide in the air, the nature of the vegetation, and the land configuration. However, much of this data is quite uncertain. Modern climate models have been used to estimate what the Eocene climate was like, but they are complicated to use, hard to understand, and in some ways are tuned to the present climate. Here we use a simpler, more flexible climate model to simulate the Eocene climate and examine how differences in the CO_2 concentration, land surface properties, ocean heat transport, and cloud extent and thickness affect the simulated climate. We find that, while increased CO_2 is a necessary condition to achieving an Eocene climate, different combinations of surface albedo, cloudiness, and surface heat capacity of land can lead to simulations that are within the proxy uncertainty range of the majority of proxy data, including the reduced seasonality of Arctic land temperatures.

1. Introduction

The early Eocene epoch featured one of the warmest climates over the last 100 million years, with global-mean temperatures some 13°C higher than today (Burke et al., 2018). In addition to its intrinsic interest, the climate of the Eocene may provide lessons for our future as the warmest simulations of the high emission scenarios lead to similar levels of warming by 2,300 (Burke et al., 2018, e.g.). The carbon dioxide (CO_2) concentration during the Eocene is rather uncertain, but estimates usually put it at between about 1,200 and 2,500 ppm, which is approximately 4–9 times pre-industrial levels (Anagnostou et al., 2020). We use these estimates for our study, other estimates of Eocene CO_2 concentrations are more constrained, with Rae et al. (2021) estimating levels at 3.7–6.8 times 300 ppm with 95% certainty. For comparison, the CO_2 concentration in 2021 was about 415 ppm. It is these increased levels of CO_2 that are almost certainly the primary reason for the warm temperatures of the Eocene.

The Eocene equator-to-pole surface temperature gradient is harder to understand, for this was remarkably low with annual-mean temperatures around 35°C at the equator and 15°C at high latitudes (Zhu et al., 2019), compared to 28°C and −10°C respectively today. Furthermore, the high-latitude land surface temperature seasonality was much reduced, with winter temperatures seemingly above 0°C (even over land) and summer temperatures around 25°C in Arctic Canada at 79°N (Eberle et al., 2010). The same rough location today (Ellesmere Island) has an

average winter temperature of −40°C and an summer temperature of 3°C. That is to say, not only was the Eocene climate much warmer than that of today, but the warming was amplified at high latitudes and further amplified in winter. A similar polar amplification effect occurs in simulations of anthropogenic global warming (Holland & Bitz, 2003) and the mechanisms of that are now becoming more clear, as reviewed by Taylor et al. (2021). While the surface albedo feedback from melting snow and sea ice is an important component of polar amplification in today's climate, models show the amplification even when this process is turned off (Graversen & Wang, 2009, e.g.). This is mainly due to the increase in atmospheric humidity, which leads to an increase in greenhouse effect and an increase in moist atmospheric energy transport, both of which produce a surface-enhanced warming in the absence of convection at high latitudes (Cronin & Jansen, 2016; Henry et al., 2021).

The Eocene picture was confused because early proxy reconstructions of Eocene climates suggested that temperatures at low latitudes increased far less than temperatures at high latitudes, so much so that climate models struggled to represent the apparently much reduced equator-to-pole temperature gradient (Huber et al., 2003, e.g.). However, the reduction in meridional temperature gradient seems to have been overestimated, with more recent estimates of tropical temperatures indicating that low-latitude temperatures were higher than was previously estimated (Pearson et al., 2007), even if still increasing less than high-latitude temperatures. Recent climate models now show a reasonable match with Eocene proxies in surface temperature gradient (Huber & Caballero, 2011; Lunt et al., 2021) at least on the annual average, although the level of CO_2 that climate models require to reproduce Eocene temperatures is somewhat higher than the proxies suggest. The required level of CO_2 would be lower if there were an increase in absorbed solar radiation (i.e., a reduced planetary albedo) and that might be achieved, for example, through a decrease in aerosol production leading to a decrease in cloud condensation nuclei and a reduction in cloud cover (Carlson & Caballero, 2017; Kiehl & Shields, 2013). The warming from CO_2 could also potentially lead to a reduction in cloud cover which reduces the planetary albedo (Zhu et al., 2019). However, there is still considerable uncertainty as to whether these effects are plausible and sufficient.

Even supposing that annual average Eocene temperature can be reproduced by climate models, difficulty arises when trying to understand the seasonality of Arctic temperatures. Various proxies (Eberle et al., 2010; Greenwood & Wing, 1995) indicate a much lower seasonal variation of temperature and suggest that, even over land, temperatures did not fall below 0°C for extended periods of time. Various mechanisms have been proposed to increase Arctic surface warming in climate models, some of which may also decrease Arctic land temperature seasonality. These include increased stratospheric clouds (Sloan & Pollard, 1998), an Arctic convective cloud feedback (Abbot & Tziperman, 2008), and Arctic low land clouds (Cronin et al., 2017; Hu et al., 2018), but how these mechanisms quantitatively fit in the overall picture of the Eocene climate is less well understood. Thus, whereas recent model simulations of the early Eocene, as described by Lunt et al. (2021), consistently ascribe the general increase in temperature to increased levels of CO_2 (as expected), the mechanisms of polar amplification and winter warmth are less clear. Even in cases where aspects of the simulations match the proxies, we do not always understand why: for example, to what degree is the dominant effect one of a change in cloud cover or type, or a change in surface boundary condition, or a change in the general circulation, or some other effect? Not only is understanding such a climate challenging in itself, but it may also inform our understanding of potentially warm future climates. Tierney et al. (2020), for example, argue that since the Equilibrium Climate Sensitivity (ECS) increases as the base state climate warms from today's value, modeling the Eocene climate can provide key constraints on the range of plausible ECS values.

Our goal in this paper is to clarify the conditions required to reproduce an Eocene climate, with particular attention to the seasonal cycle and the maintenance of relatively warm winters over Arctic land. To this end we use a very flexible general circulation model (GCM), configured with Eocene land and topography, that enables us to independently vary CO_2 levels, cloud distributions, ocean heat transport, and various land-surface parameters. We thereby seek to understand how these processes, separately and together, affect the global-mean temperature, the equator-to-pole surface temperature gradient, and the seasonality in Arctic land temperature. We begin with a description of the model itself (Section 2), and follow this with a description of experiments in which we change the surface boundary conditions (Section 3), the clouds (Section 4), the land surface heat capacity (Section 5), and ocean heat transport (Section 6).

2. Model and Reference Simulations

We construct our models using the Isca climate modeling framework (Vallis et al., 2018) configured with no sea ice, a slab mixed-layer ocean, and a simple representation of land hydrology, and topography with Eocene continental outlines taken from Herold et al. (2014). Meridional ocean heat transport is represented by imposing an ocean surface heat flux (q-flux), which allows us to study the effects of varying its magnitude, as described further in Section 6. The cloud scheme (Liu et al., 2020) diagnoses large-scale clouds primarily from relative humidity with the addition of a simple representation of marine low stratus clouds (which have a large shortwave effect) and a "freeze-dry" adjustment that reduces the cloud cover under the very dry conditions in polar regions. Stratospheric cloud changes (for which the prediction is particularly uncertain) are prescribed instead of dynamically predicted. As with our representation of the ocean, our purpose is to explore the effects of changing uncertain parameters and amounts rather than to present a single "best" simulation, and more detail is present in Section 4.

The model has 40 pressure levels and the model top is at 3 Pa; this is comparable to many other climate models (Lunt et al., 2021) and is generally sufficient to adequately resolve the main tropospheric and stratospheric processes for our purposes. Simulations are run at spectral T42 resolution, which corresponds to approximately 2.8° resolution at the equator. The stratospheric ozone distribution is taken from Jucker and Gerber (2017). We impose a seasonal cycle of insolation and use the comprehensive SOCRATES radiation scheme for both solar and infra-red radiation (Manners et al., 2017; Thomson & Vallis, 2019), which maintains good accuracy for CO_2 levels up to a factor of 16 or more than present values. The surface albedo is set to 0.075 over ocean and 0.15 over land which is similar to comprehensive model simulations of the Eocene (Lunt et al., 2021). Land also differs from oceans by its heat capacity, which we set (in our control simulations) to 0.2 m equivalent water depth for continents (Merlis et al., 2013) and 20 m for oceans, and by the roughness constant, which is set to be 10 times higher over land than ocean. The ocean is assumed to have an infinite supply of water. A land evaporative resistance parameter (β in Equation 10 of Vallis et al. (2018)) is used to model the limited water availability of land, which sets the fraction of the surface evaporation flux to be a function of what it would have been if there was an infinite supply of water. If the parameter is set to 1, then the surface evaporation flux over land is like that over ocean; here, we set this parameter to 0.5. We use the Eocene's land distribution (the contour is visible in Figure 1), and notice that most modern day continents are recognizable, though the continental configuration may have an impact on ocean circulation. Convection is calculated using a simplified Betts–Miller convection scheme (Frierson, 2007). Large-scale condensation is parameterized such that relative humidity does not exceed one and condensed water immediately returns to the surface, and the cloud distribution is not directly coupled to the precipitation. There is no representation of snow in this model, hence it does not impact surface properties, such as albedo, evaporative resistance, or heat capacity.

We first describe five reference simulations with a fixed set of control parameters in which CO_2 concentrations are set to 300 ppm, 900 ppm (3×300 ppm), 1,800 ppm (6×300 ppm), 2,700 ppm (9×300 ppm), and 3,600 ppm (12×300 ppm). Following that, we discuss a set of experiments where the surface albedo and land evaporative resistance are modified, a set where we prescribe various high-latitude cloud distributions, a set where we reduce the land's surface heat capacity, a set where we test the importance of ocean heat transport by prescribing a meridional heat transport in the slab ocean. And, finally a set where we simulate a change in vegetation with an increase in land heat capacity, a decrease in albedo, and an increase in land evaporative resistance. The list of experiments, parameters explored, relevant manuscript sections, and abbreviations used in the figures are summarized in Table 1.

Figure 1 shows the annual-mean and winter (December, January, and February mean (DJF)) surface temperature for the 300 and 3,600 ppm simulations. At 300 ppm, the winter temperatures reach below −30°C in parts of the Arctic land whereas at 3,600 ppm, the winter temperatures are above zero almost over the whole Arctic land surface. At 2,700 ppm the temperatures fall below zero for periods in winter, as seen in Figure 2. The global-mean surface temperature of the 300, 900, 1800, 2700, and 3,600 ppm reference simulations is 288.4, 291.3, 293.5, 295.5, and 297.6 K respectively. The ECS is given by the surface temperature change from a doubling of CO_2, hence we normalize the surface temperature change by $\log_2(\Delta CO_2)$ where ΔCO_2 is the increase in CO_2 between two experiments, as the CO_2 forcing is approximately proportional to the logarithm of its concentration. The ECS is 1.8, 2.3, 3.3, and 5.1 K, respectively, for these simulations. This increasing climate sensitivity is consistent with what Caballero and Huber (2013) found, for example, The climate sensitivity for the initial increase in CO_2

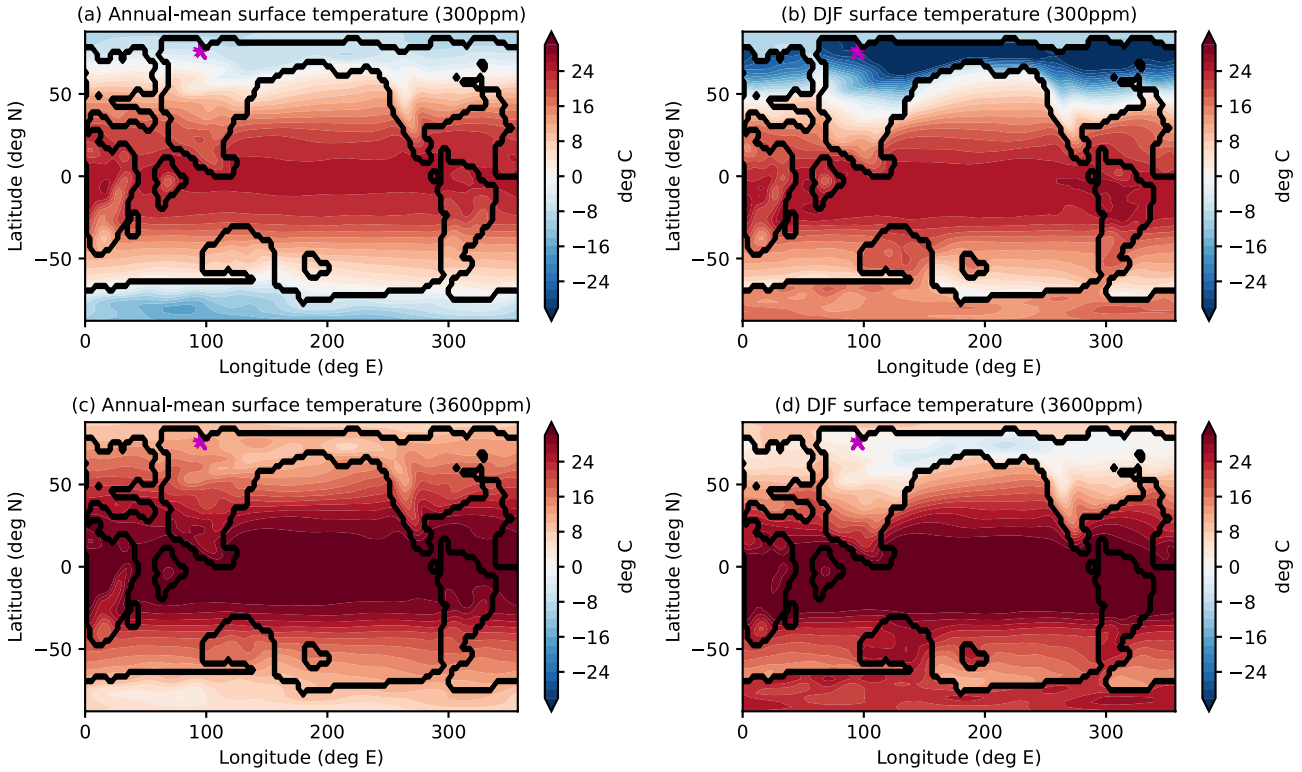

Figure 1. Surface temperatures in control simulations with present-day and very high CO_2 levels. Annual-mean surface temperature (a, c) and December-January-February (DJF) surface temperature (b, d) for the 300 ppm (a, b) and 3,600 ppm (c, d) simulations, as labeled. Purple stars represent the location used in Figure 2c.

(1.8 K) is somewhat less than typical ECS estimates for the modern climate (e.g., 2.3–4.5 K from Sherwood et al. (2020)). This is probably due to the absence of sea ice, the melting of which leads to a positive feedback, and a relatively stabilizing cloud feedback, suggesting that our climate simulations may be biased cold at higher CO_2 values. Additionally, the polar amplification factor, calculated as the ratio of warming poleward of 60° and warming between 30° North and South, is 4.7, 4.0, 3.7, 2.7 for each increase in CO_2. These polar amplification factors are low compared to comprehensive models which have a multi-model mean of 11.9 (Lunt et al., 2021), but these include both CO_2-induced changes and changes in the boundary conditions (such as the removal of the ice

Table 1
List of GCM Experiments With Type of Experiment, the Explored Parameter Range, the Relevant Section Number, and the Abbreviation Used in the Figures

Experiment type	Parameter range	Section	Abbreviation
Control simulations	CO_2 set to 1,3,6,9,12x preindustrial level (300 ppm)	2	CO_2 only
Surface albedo	Set to 0.05 over ocean and 0.10 over land (instead of 0.075 and 0.15 respectively)	3	alb 0.5
Land evaporative resistance	Set to 1 instead of 0.5	3	evap 1
High-lat ocean high clouds	Cloud fraction min set to 0.25, 0.5, and 0.75 between 300 and 500 hPa over high-lat ocean	4	high ocean
High-lat land low clouds	Cloud fraction min set to 0.35 and 0.7 between 600 and 1,000 hPa over high-lat land	4	low land
Increased stratospheric clouds	Cloud fraction min set to 0.2 between 0 and 200 hPa over high-latitudes	4	strat
No stratospheric clouds	Cloud fraction max set to 0 between 0 and 200 hPa over high-latitudes	4	no strat
Land surface heat capacity	Set to 0.1x ocean surface heat capacity (instead of 0.01)	5	0.1 landhc
Vegetation change	Increase land heat cap (0.1), decrease albedo (0.05/0.1), increase land evap resistance (1)	5	veg
Ocean heat transport	0,1,2x prescribed meridional ocean heat transport	6	0,1,2x oht

Note. Note that each experiment type has been run with CO_2 concentrations set to 1, 3, 6, 9, and 12 times preindustrial levels.

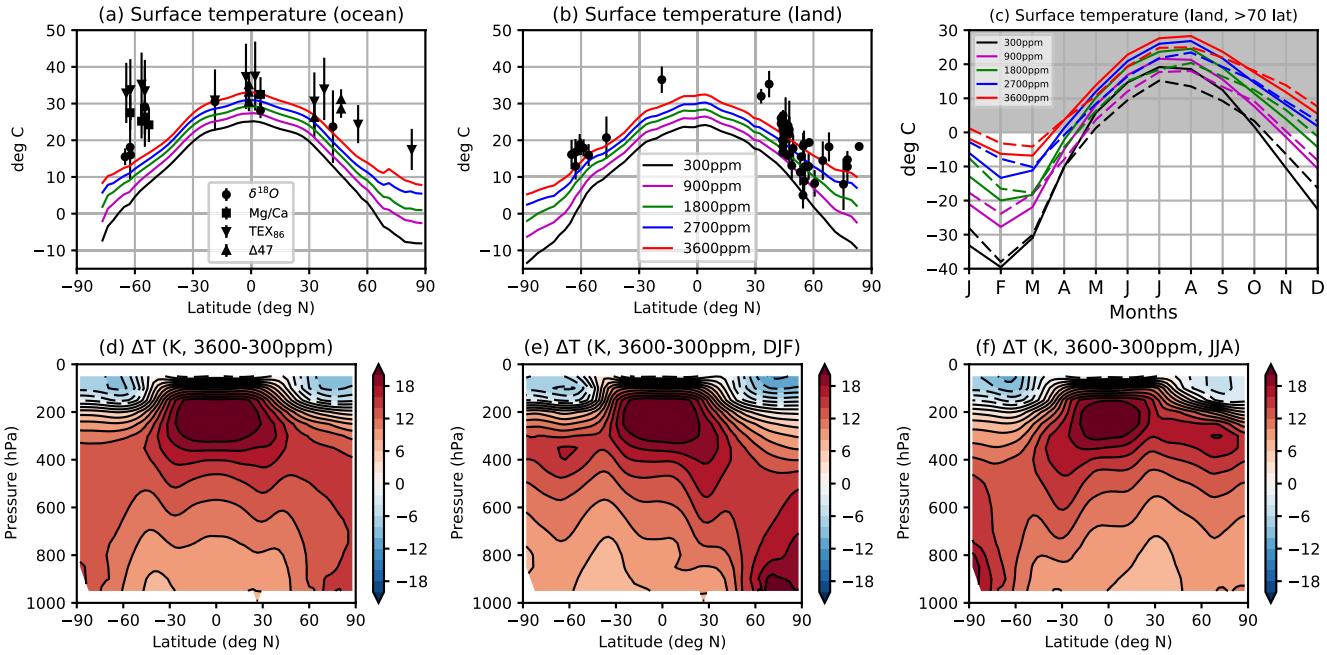

Figure 2. Surface temperature for various Eocene simulations. Annual-mean ocean (a) and land (b) surface temperature for control simulations (all CO_2 levels) compared with proxies (symbols). The root mean squared error (RMSE) between model and proxy values is 17.8, 15.1, 12.9, 11.4, and 9.8 K for ocean, and 13.1, 9.4, 7.0, 5.4, and 4.7 K for land, for the 300, 900, 1800, 2700, 3,600 ppm reference simulations respectively. Seasonality of Arctic (poleward of 70° North) land surface temperature (solid) and for location pinned by the star in Figure 1 (dashed) for reference simulations (c), with proxy-derived estimate in gray. The gray represents the values derived from Eberle et al. (2010). The proxy values for ocean surface temperatures are compiled by Zhu et al. (2019). The land surface temperatures are from Huber and Caballero (2011). Atmospheric temperature change for the difference between the 300 and 3,600 ppm simulations in the annual-mean (d), December-January-February (DJF) (e), and June-July-August (JJA) (f), as labeled.

sheets). Hence a higher sensitivity model would have higher tropical temperatures and even higher high-latitude temperatures, thus better matching the proxies for ocean surface temperatures (Figure 2a).

The zonal-mean land and ocean surface temperature are compared with proxies (Barrera, 1991; Bijl et al., 2009, 2013; Cramwinckel et al., 2018; Creech et al., 2010; Evans et al., 2018; Frieling et al., 2014; Hines et al., 2017; Hollis et al., 2009, 2012, 2015; Inglis et al., 2015; John et al., 2008; Keating-Bitonti et al., 2011; Kozdon et al., 2011; Lu & Keller, 1993; Pearson et al., 2007; Sluijs et al., 2006; Stott et al., 1990; Tripati et al., 2003; Zhu et al., 2019) in Figures 2a and 2b. The land surface temperatures are from Huber and Caballero (2011). A more recent data set can be found in Hollis et al. (2019), however their results are similar to those of Zhu et al. (2019) and comparing against this data set would not change the overall interpretation of our results. The annual-mean surface temperature is more or less within the proxy range for land for CO_2 concentrations above 1,800 ppm (the root mean squared error (RMSE) is 13.0, 9.4, 7.0, 5.4, and 4.7 K for the 300, 900, 1800, 2700, and 3,600 ppm simulations respectively). While some proxy ocean temperature points are warmer than all simulations, simulations with CO_2 concentration above 2,700 ppm yield a reasonable match with proxies (the RMSE is 17.8, 15.1, 12.9, 11.4, and 9.8 K for the 300, 900, 1800, 2700, and 3,600 ppm simulations respectively). The seasonality of Arctic land temperature (Figure 2c) shows that winter land temperatures are more sensitive to an increase in CO_2 (Henry & Vallis, 2021b) and that even at 3,600 ppm, the land temperature is still below 0°C in winter. We use an average over all land poleward of 70° North (solid). As most proxies are from samples taken on coastal areas, we compare this average with the seasonality for a single grid point on the coast (dashed), indicated by a star in Figure 1. The difference with the average of all land temperatures (solid) is modest, which is perhaps surprising. Choosing other points or comparing near-surface temperatures also showed a modest difference. Moreover, a comparison of our 3,600 ppm reference simulation with the terrestrial cold month mean temperatures from Huber and Caballero (2011, their figure 6) does show a fairly good match (Figure 3). The 2,700 ppm simulation is a little cool, and a CO_2 level of 3,600 ppm is higher than most Eocene CO_2 estimates, hence suggesting that in this configuration our model's sensitivity is rather low, as is further discussed later. With a higher sensitivity model we would get a better match in the annual-mean and also a better match in cold month mean land temperatures at

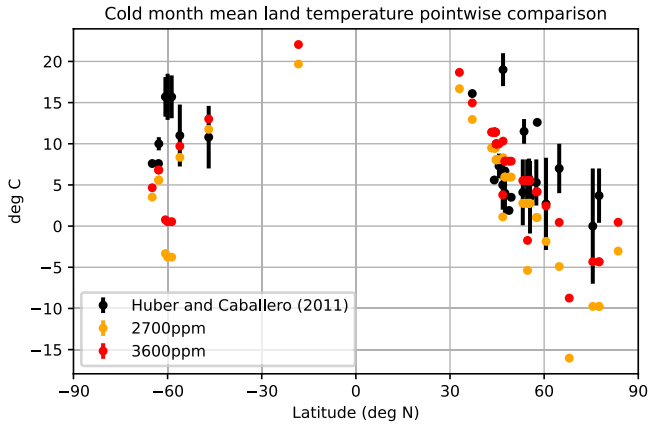

Figure 3. Pointwise comparison of cold month mean land surface temperatures between the proxy estimates taken from (Huber & Caballero, 2011) (black) and points taken from our reference 2,700 ppm (orange) and 3,600 ppm (red) simulations.

high latitudes, which typically increase faster than the global-mean (Henry & Vallis, 2021b). The difference is not so marked that qualitatively new physics is needed, but that cannot be said to have been definitively established here. The atmospheric temperature change in the Arctic is surface enhanced in winter and top-heavy in the summer (Figures 2d–2f). In summer, the land surface gets warm enough to trigger convection which pins the atmospheric temperature to the moist adiabat, whereas in winter the absence of convection leads to surface-enhanced warming. This was explained for similar simulations without clouds in Henry et al. (2021).

As noted in the introduction, atmospheric models produce polar amplification—meaning an enhanced warming at and near the surface at high latitudes—when CO_2 is increased, even without changes in ice cover and our model has no representation of sea or land ice. To understand this, first note that the presence of convection in the tropics pins the atmospheric temperature profile there to the moist adiabat; this means the temperature increase is largest in the upper troposphere and lowest near the surface, giving a negative lapse rate feedback on surface temperature in the tropics. In contrast, at high latitudes the overall increase in water vapor (due to a higher temperature and increase in meridional moisture transport) leads to surface-enhanced atmospheric temperature change at high latitudes and so a positive lapse rate feedback (Henry et al., 2021). The consequence is that, even if the mid-atmosphere meridional temperature gradient were to remain unchanged, there will be an effective low-level polar amplification. If sea-ice were present in the model, its loss would make the lapse rate feedback even more positive (Feldl et al., 2020).

In addition to polar amplification, the increased temperatures that results from the additional CO_2 forcing alone reduces the seasonality of Arctic land temperature due to the small heat capacity of land (Henry & Vallis, 2021b). This effect arises from the nonlinearity of the temperature dependence of surface longwave emission, which is proportional to σT_S^4 where T_S is the surface temperature. Surfaces at low temperature need to warm more than those at high temperature in order to achieve the same increase in emission, leading to a larger increase in surface temperature in winter than in summer. The seasonality is naturally larger over land than ocean, because of the smaller heat capacity of the land, so the effect is much more pronounced over land. Increases in evaporation over land in summer also contribute to the winter-amplified pattern of surface temperature change. Indeed, surface evaporation is calculated as proportional to the difference between saturation vapor pressure calculated using the surface temperature and the humidity of the lowest atmospheric level (Vallis et al., 2018), and the former increases faster than the latter with warming in summer over land (Henry & Vallis, 2021b).

The combined effects of polar amplification and a reduction in seasonality of Arctic land temperature are observed in all high-CO_2 simulations, regardless of the presence or otherwise of sea ice or clouds. The same effect is present in extended RCP8.5 simulations before and after sea ice disappears in comprehensive models (Henry & Vallis, 2021b). These effects are the dominant mechanisms leading to increased high-latitude surface temperatures over land in winter, and go a long way toward explaining the proxy measurements indicating the lack of extended periods of freezing in winter. However, in and of themselves they may be insufficient for us to be confident we have good agreement with the proxies, and for that reason we explore what additional effects may be important.

3. Modifying Surface Boundary Conditions

We now explore the effects of changing the surface boundary conditions. In one set of experiments, the surface albedo is set to 0.05 over ocean and 0.10 over land (instead of 0.075 and 0.15 respectively in the control simulations), simulating a change in planetary albedo which could occur due to changes in cloud distribution or in surface properties such as ice cover and vegetation, but is implemented as a change in surface albedo for convenience. And in another set of experiments, the evaporative resistance parameter is set to 1 enabling the land to evaporate as efficiently as the ocean, mimicking a swamp-like surface. Figures 4a and 4b show the ocean and land surface temperature respectively for these simulations. Reducing the albedo means that, at 2,700 ppm, the surface

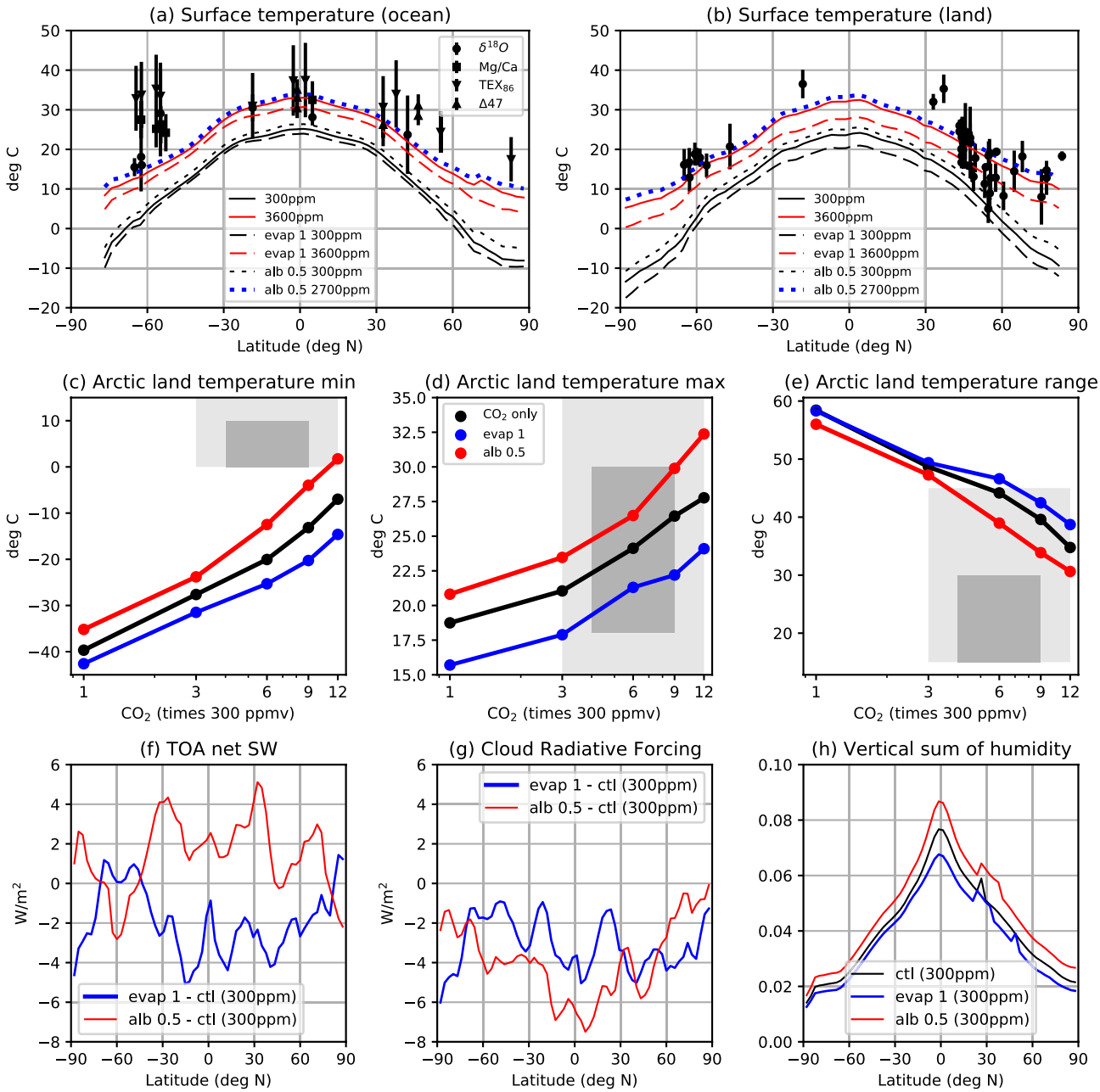

Figure 4. Simulations with modified land evaporative resistance and modified surface albedo. Ocean (a) and land (b) annual-mean surface temperature. The root mean squared error between model and proxy values is 17.8, 9.8, 19.0, 11.6, 16.3, 8.9 K for ocean, and 13.1, 4.7, 15.7, 6.6, 10.9, 4.7 K for land, for the 300 and 3,600 ppm reference simulations, the 300 and 3,600 ppm "evap1" simulations, and the 300 and 2,700 ppm "alb05" simulations respectively. Seasonality of Arctic land temperature (c, d, and e). Difference in annual-mean top-of-atmosphere net shortwave radiation (f) and cloud radiative effect (g), and vertical sum of atmospheric humidity (h). In panels (a and b), the proxy values for ocean surface temperatures are compiled by Zhu et al. (2019) and the land surface temperatures are from Huber and Caballero (2011). In panels (c, d, and e), the gray represents the values derived from Eberle et al. (2010), and the light gray is a larger interval to account for the uncertainty in proxy values.

temperature is similar to the reference simulation at 3,600 ppm and matches the proxies (Figures 4a and 4b) (the RMSE of the low albedo simulation at 2,700 ppm is 8.9 K for ocean and 4.6 K for land compared to 9.8 and 4.7 K respectively for the 3,600 ppm reference simulation). The monthly temperature minimum, maximum, and temperature range of Arctic (poleward of 70° North) land are given in Figures 4c–4e respectively. The dark gray boxes denote the proxy-derived values (Eberle et al., 2010), and the light gray boxes are a feasible extension of these proxy-derived values as they are quite uncertain. The Arctic land temperature minimum only reaches above

0°C for 12 × 300 ppm and a lower surface albedo, the Arctic land temperature maximum however is within the proxy-derived range for all simulations.

Figures 4f and 4g show the difference in top-of-atmosphere (TOA) net shortwave radiation and cloud radiative effect respectively between the reference 300 ppm simulation and the increased land evaporation (blue) and decreased albedo (red) 300 ppm simulations. Figure 4h shows the vertical sum of specific humidity for the same simulations. Decreasing the surface albedo leads to more shortwave radiation being absorbed at the surface, hence higher net shortwave radiation at the TOA (Figure 4f). The shortwave cloud radiative effect depends on the albedo difference between the cloud and the surface, hence decreasing the surface albedo also leads to a tropically-amplified decrease in the cloud radiative effect (Figure 4g) as the clouds' reflection of sunlight contributes more to the planetary albedo. Increasing surface evaporation over land leads to more low clouds over land and a more negative cloud radiative effect and less net shortwave radiation at the TOA (Figures 4f and 4g, blue). Note that the decrease in cloud radiative effect and net shortwave radiation at the TOA are generally higher at latitudes with more land (Figures 4f and 4g, blue). Finally, the atmosphere is moister in the simulation with a smaller surface albedo and less moist in the increased evaporation simulation (Figure 4h).

In summary, both changing the surface albedo and increasing land surface evaporation affect the amount of absorbed solar radiation at the TOA, hence affect the global mean and Arctic warming, as well as atmospheric humidity. Decreasing the surface albedo increases absorbed solar radiation, warms the planet, and increases atmospheric humidity. Increasing surface evaporation increases the amount of low clouds over land. This cools the climate in the tropics and midlatitudes due to an increase in the shortwave cloud radiative effect, which in turn leads to a reduction in specific humidity over the whole planet including the Arctic (Figure 4h). Hence there is a reduction in the greenhouse effect and a reduction in Arctic land temperature even in winter when the shortwave cloud radiative effect is not active. Note that if the low clouds are increased only over the Arctic land, this leads to warming in winter (as shown in Section 4) as there is an increase in the greenhouse effect from the additional clouds but no reduction in atmospheric humidity.

4. Effect of Various Arctic Cloud Configurations

The parameterization of clouds is one of the most uncertain aspects of climate modeling, especially but not only for climates different from that of today. Even the most sophisticated cloud scheme cannot be guaranteed to give realistic results for the Eocene and we therefore explore how variations in cloud parameters and amounts affect the climate at various levels of CO_2.

We first look at the effects of some parameter changes in the cloud scheme. In our scheme the effective radius of liquid and ice cloud droplets is set to 14 and 25 microns respectively, and the in-cloud liquid water mixing ratio is set to 0.18 g/kg, and these are kept fixed, as in Liu et al. (2020). The cloud fraction is then estimated based on the relative humidity, and a “freeze-dry” scheme adjusts that estimate for the very cold and dry conditions of the polar regions. Since these regions are a focus of this study, we test the sensitivity of the simulations to the freeze-dry scheme parameters. Specifically, if the cloud fraction is below a given threshold, the freeze-dry scheme further decreases the cloud fraction linearly as a function of the water vapor content. We explore the effect of changes to this threshold specific humidity value by setting q_0 to 0.003 kg/kg and 0.012 kg/kg instead of its 0.006 kg/kg reference value (see Figure 4b of Liu et al. (2020)) for different levels of CO_2. Figure 5 shows that changing q0 to 0.003 kg/kg increases the Arctic land winter temperature making it larger than −2°C year-round for the 3,600 ppm simulation. However, these changes are smaller than the other changes we impose, which are described below. Hence the freeze-dry parameter is kept at its reference value for all the experiments presented below.

Regarding cloud regimes, Abbot and Tziperman (2008) argue that deep convection could occur over high-latitude oceans in winter when they are ice-free (as is the case during the Eocene); if so, the consequent increased longwave cloud radiative effect could help account for the warm Arctic winters. Moreover, Cronin et al. (2017) argue that, as relatively warm maritime air masses are advected over Arctic land in winter the low-cloud optical thickness increases thereby suppressing surface cooling and amplifying winter Arctic land warming. These results are supported by single column model simulations (Cronin & Tziperman, 2015) and GCM simulations (Hu et al., 2018). Finally, for high enough CO_2, Arctic stratospheric clouds can form in winter, which were hypothesized to be important in maintaining warm Arctic winters (Sloan & Pollard, 1998). In order to test these

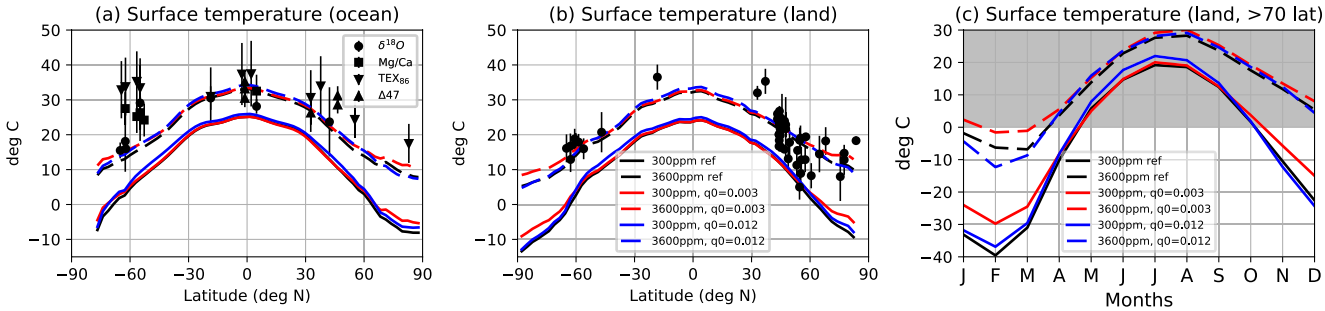

Figure 5. Cloud parameter sensitivity experiment. Ocean (a) and land (b) annual-mean surface temperature, and seasonality of Arctic land temperature (c) for reference experiments (black) and for experiments where cloud scheme parameter q_0 is set to 0.003 kg/kg (red) and 0.012 kg/kg (blue) instead of the 0.006 kg/kg reference value.

various hypotheses as to how clouds affect Arctic warming, we prescribe increased high clouds over the Arctic ocean year-round in one set of simulations, and we prescribe increased low clouds over Arctic land year-round in another set of experiments. Additionally, we prescribe increased Arctic stratospheric clouds in one set of experiments and suppress them in another. In this type of experiment, at every model timestep the minimum cloud fraction is set to a given value for a specified latitude and pressure range, such that the cloud fraction can exceed but not be below the given value. In the case where clouds are suppressed, we set the maximum value for cloud fraction for the specified latitude and pressure range.

The "low land" experiments consist in increasing the amount of low cloud over high-latitude land by setting the cloud fraction minimum to be 0.35 and 0.7 for land surfaces poleward of 60° between 600 and 1,000 hPa, values that are generally consistent with those presented in Hu et al. (2018). For comparison, the annual-mean zonal-mean cloud fraction in the control 300 ppm simulation is shown alongside the cloud fraction in the 0.35 and 0.7 cloud fraction minimum simulations in Figures 7a–7c. The Arctic land temperature minimum, maximum, and range are given in Figures 7d–7f. The light and dark gray boxes are the same as in Figure 4. Low clouds normally have a larger effect in the visible than in the infra-red (discussed more below), and thus tend to lower the summer temperatures, as seen in Figure 7e. Low clouds also have a warming greenhouse effect which increases the winter minimum temperature, but this effect diminishes at high CO_2 as the longwave opacity of the atmosphere increases. The net effect is to reduce the seasonality of the Arctic land temperature to being almost within the proxy bounds of temperature at 9 × 300 ppm and 12 × 300 ppm, although the minimum is still too low. The Arctic land temperature maximum is generally within proxy-derived values for levels of CO_2 above 3 × 300 ppm.

The radiative effect of the imposed clouds is the difference in the top-of-atmosphere radiation budget between all-sky and clear-sky conditions with the temperature profile of the all-sky conditions. The difference between the radiative effect with the prescribed cloud described in the previous paragraph and the reference simulation is shown in Figure 7g for the 300 ppm simulations. As is well known, low clouds generally have a larger effect in the visible than in the infrared, and hence have a cooling effect, particularly when insolation is large as in summer. In winter at high latitudes, when the insolation is small, the infra-red dominates and the additional low clouds have a warming effect, albeit a small one. Thus, the net effect of the additional low clouds is to reduce the magnitude of the seasonal cycle. Even though the shortwave effect in summer is larger that the infra-red effect in winter, the impact on the land temperature is actually larger in winter than in summer (Figure 7h), because of the "winter-warms-more" mechanism discussed in Henry and Vallis (2021b). At high CO_2, the presence of additional low clouds over land has little effect on Arctic winter land temperatures because the longwave opacity of the Arctic atmosphere is already high due to high cloudiness (Figure 6), CO_2, and water vapor (not shown). Hence, at high CO_2, the "winter-warms-more" effect is still present, but the radiative effect of additional clouds in winter is a lot smaller than at low CO_2. Adding even more low clouds (cloud fraction higher than 0.90 e.g.) at levels of CO_2 compatible with Eocene proxies (4–9x 300 ppm) may help with reconciling winter surface temperatures with their proxy values. Note that adding low clouds reduces summer temperatures at all CO_2 levels through its shortwave effect (Figure 7e).

The "high ocean" experiments consist in increasing high clouds over high-latitude ocean by setting the cloud fraction minimum to 0.25, 0.5, and 0.75 for ocean surfaces poleward of 60° between 300 and 500 hPa. For comparison, the annual-mean zonal-mean cloud fraction in the control 300 ppm simulation is shown alongside

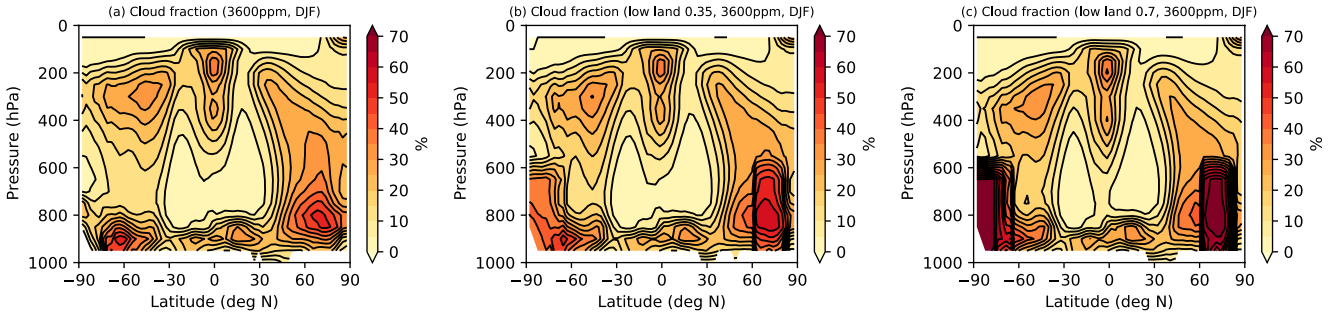

Figure 6. Zonal-mean cloud fraction in December, January, and February (DJF) for the control (a), 0.35 (b) and 0.7 (c) minimum low cloud fraction over Arctic land simulations at 3,600 ppm.

the cloud fraction in the 0.25 and 0.75 cloud fraction minimum simulations in Figures 8a–8c. The Arctic land temperature minimum, maximum, and range are not changed much (Figures 8d–8f), despite the large increase in high clouds in the 0.75 experiment (Figure 8c). High clouds generally have a warming effect as the increase in longwave opacity is larger than the increase in reflected sunlight and because the reference climate has a lot of low-level cloudiness (Figure 8a). The additional radiative effect of high clouds is, at least in these simulations, relatively weak in all seasons (Figure 8g). The effect is to warm in all seasons, with more warming in winter and most of that over land, because of its low surface heat capacity (Figure 8h). Using a single column model of the Arctic with clouds, Abbot and Tziperman (2008) vary CO_2 and ocean and atmospheric heat transport and find warm equilibria without sea ice and cold equilibria with sea ice. When sea ice is absent, there is more atmospheric humidity and there is convection in winter which lead to the presence of high clouds with a strong radiative effect. This feedback could then explain the exceptional Arctic warmth in high CO_2 climates. In our simulations, there is no sea ice, hence we isolate the effect of increased high clouds. And our simulations show that this effect is not enough to significantly increase Arctic surface temperatures.

Finally, the stratospheric cloud experiments consist in increasing and eliminating polar stratospheric clouds by setting the cloud fraction minimum to 0.2 and 0 respectively poleward of 60° between 0 and 200 hPa. For comparison, the annual-mean zonal-mean cloud fraction in the control 300 ppm simulation is shown alongside the cloud fraction in the no stratospheric cloud and increased stratospheric cloud simulations in Figures 9a–9c. The Arctic land temperature minimum, maximum, and range are almost unchanged (Figures 9d–9f). This may be because the radiative effect of these clouds is very small, at least in these simulations (Figure 9g), and hence does not change the surface temperature (Figure 9h). This differs from the Sloan and Pollard (1998) results which showed that clouds with a 100% cover between 10 and 40 hPa in winter time can lead up to 20 K of local warming in regions of sea ice decline. The lack of warming in our simulations most likely comes from our less extreme increase in stratospheric clouds.

5. Modifying Land Surface Heat Capacity

In our reference simulations, the surface heat capacity of land is equivalent to an ocean mixed-layer depth of 0.2 m, with that of ocean itself being 20 m. The value of the land heat capacity is taken from Merlis et al. (2013): the product of specific heat capacity and density for soil is approximately 0.2 times that of the ocean, and the effective diffusion depth for soil is approximately 1 m for the seasonal cycle (Pierrehumbert, 2010). Hence the equivalent depth of the land "mixed layer", in terms of meters of water, is $0.2 \times 1 = 0.2$ m, a factor of 100 less than the value we use for the ocean. These values give a seasonal cycle of about the right magnitude and phase for the climate of today, though summer temperatures for the current climate have a slight warm bias because of the absence of snow in these simulations.

The characteristics of the land surface were likely quite different in the Eocene, especially at high latitudes where frozen soil and ice is replaced by abundant vegetation and possibly swamps and lakes. We therefore explore the sensitivity of our results to an increase in land surface heat capacity. Specifically, we set the mixed layer depth over land to 2 m instead of 0.2 m and to see how this affects the seasonal cycle at high CO_2 levels. The increase in the "mixed layer depth" of land to 2 m leads to an increase in the surface's heat capacity, hence it takes more time for the surface to warm up in summer and cool down in winter and the temperature is closer to

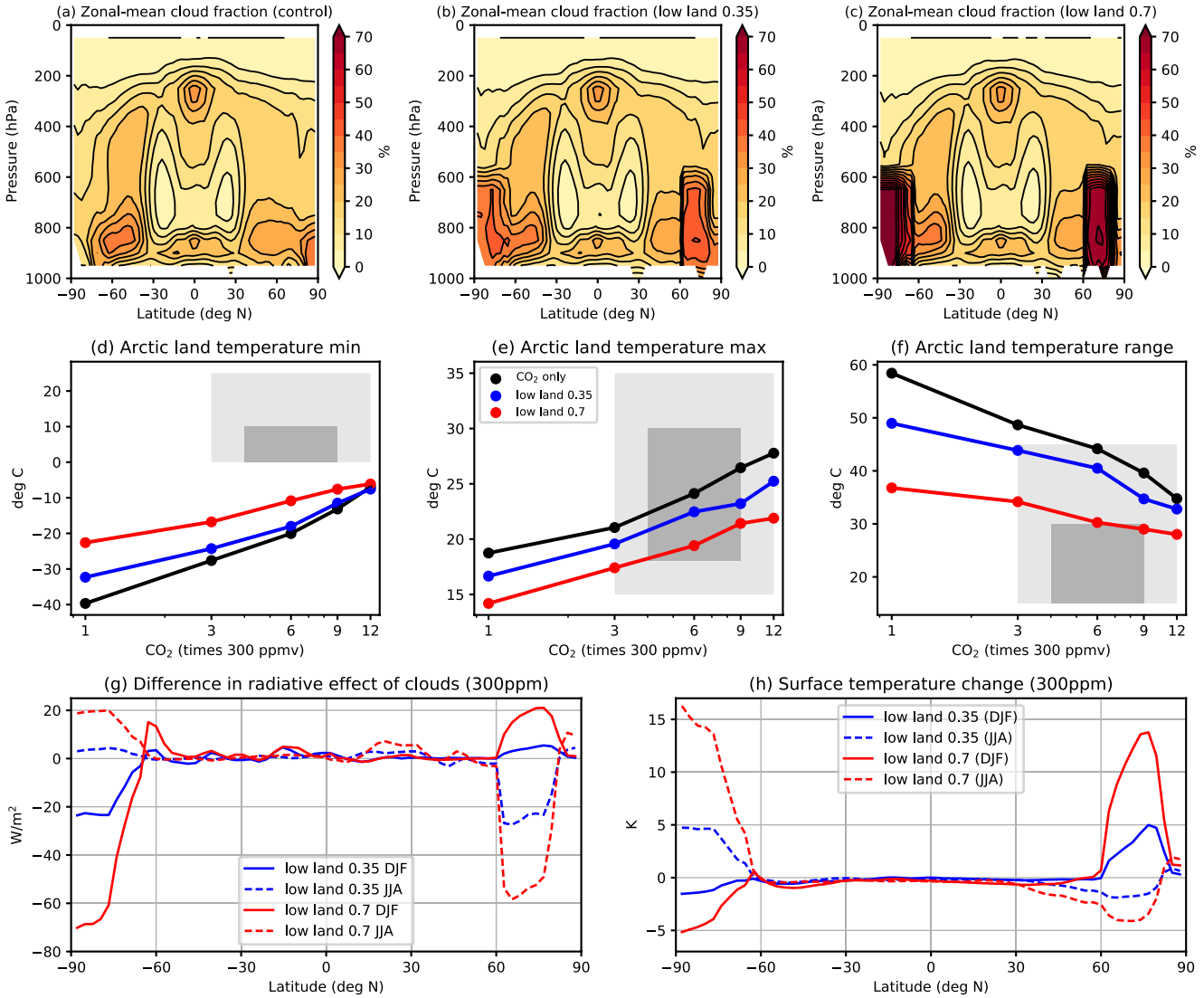

Figure 7. Prescribed additional low clouds over Arctic land experiments. Zonal-mean annual-mean cloud fraction for the control (a), 0.35 (b) and 0.7 (c) minimum high cloud fraction over Arctic ocean simulations at 300 ppm. Monthly minimum (d), maximum (e), and range (f) of Arctic land surface temperature for all three sets of simulations. The difference in radiative effect of clouds (g) and surface temperature change (h) between the prescribed cloud and control experiments at 300 ppm for Northern hemisphere winter (DJF) and summer (JJA). In panels (d, e, and f), the dark gray represents the values derived from Eberle et al. (2010), and the light gray is a larger interval to account for the uncertainty in proxy values.

its annual-mean year round. This does not substantially change the zonal-mean annual-mean surface temperature (Figures 10a and 10b compared to Figures 2a and 2b). However, the seasonal cycle of Arctic land temperature is much reduced, and almost consistent with proxies (dark gray box) at 2,700 ppm and fully consistent with proxies at 3,600 ppm (Figure 10c).

Since the increased prescribed low clouds over land led in the direction of a climate consistent with proxies (Figure 7), we also explore the combined effects of a higher land surface heat capacity with increased prescribed low clouds over land (the cloud fraction minimum is set to be 0.7 for land surfaces poleward of 60° between 600 and 1,000 hPa). Although it does not, in fact, substantially change the winter Arctic land temperature, it does decrease the summer Arctic land temperature (Figure 10c) by increasing the albedo (Figure 7g); that is, it lowers the Arctic land seasonality, which is the main stumbling block in simulations of the Eocene climate.

Further, it was previously found that changes in Arctic vegetation can lead to simultaneous changes in surface albedo and soil properties, which in turn impact water vapor, clouds, and sea ice, and potentially amplify

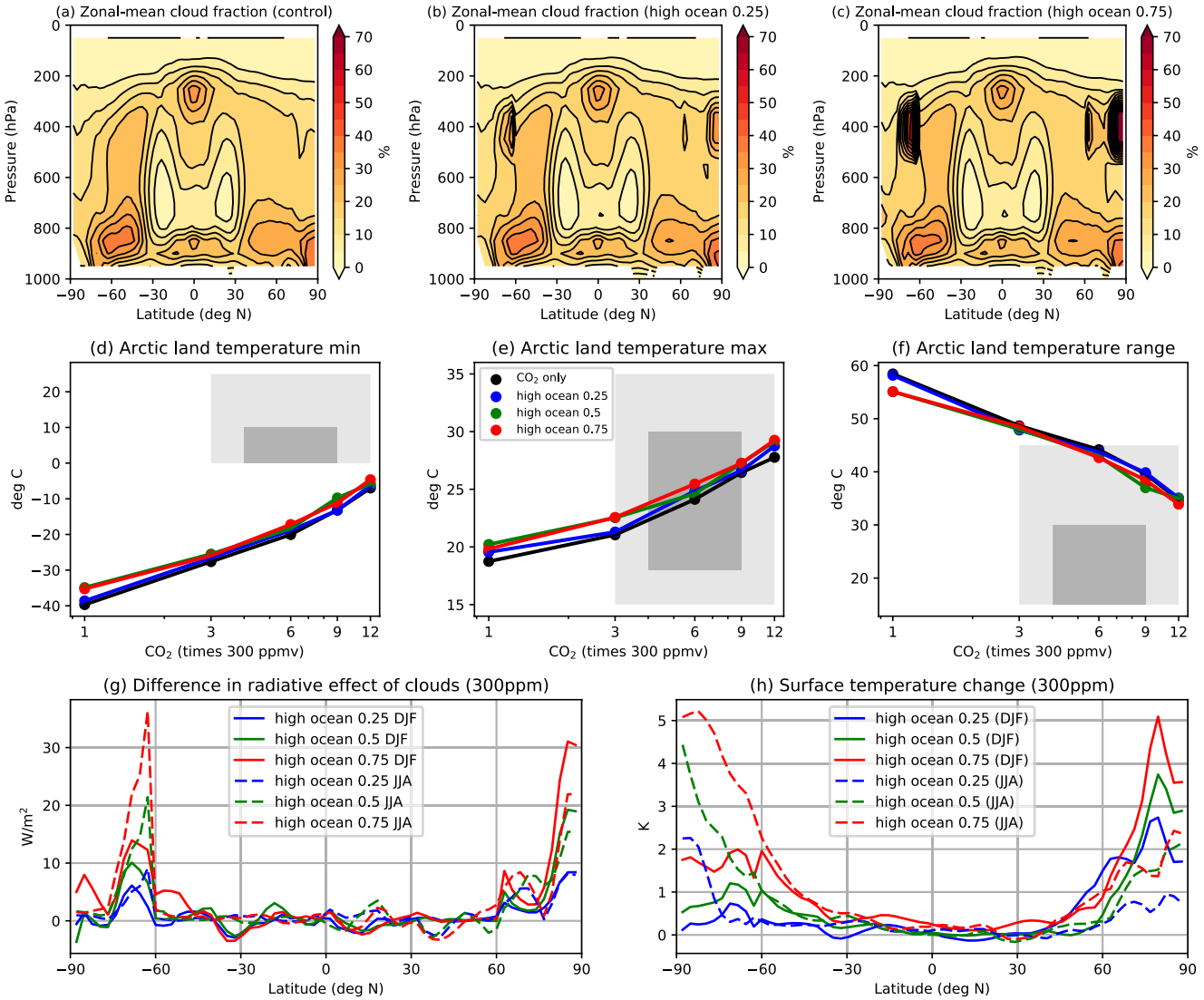

Figure 8. Prescribed additional high clouds over Arctic ocean experiments. Zonal-mean annual-mean cloud fraction for the control (a), 0.25 (b) and 0.75 (c) minimum low cloud fraction over Arctic land simulations at 300 ppm. Monthly minimum (d), maximum (e), and range (f) of Arctic land surface temperature for all four sets of simulations. The difference in radiative effect of clouds (g) and surface temperature change (h) between the prescribed cloud and control experiments at 300 ppm for Northern hemisphere winter (DJF) and summer (JJA). In panels (d, e, and f), the dark gray represents the values derived from Eberle et al. (2010), and the light gray is a larger interval to account for the uncertainty in proxy values.

high-latitude warming (Swann et al., 2010). Hence, we do an additional "modified vegetation" set of simulations, where the land heat capacity is increased from 0.01 to 0.1 times that of the ocean (same as "0.1 landhc"), the albedo is decreased to 0.05 over ocean and 0.1 over land (same as "alb 0.5"), and the land evaporative resistance is set to 1 (same as "evap 1"). The increased land heat capacity decreases the seasonality of Arctic land, the albedo decrease modestly decreases the seasonality, and the land evaporative resistance increase modestly increases the seasonality. Combined, these three factors decrease the seasonality and make it very nearly within proxy bounds (Figure 10c, green), even for 2,700 ppm. This is most likely due to the dominant role of the large increase in land surface heat capacity. Finally, we do one last simulation with "modified vegetation" and additional low clouds over land for 2,700 ppm (Figure 10c, magenta). This simulation has a similar seasonality to the simulation with low land clouds and increased land surface heat capacity (Figure 10c, red), but with slightly higher winter temperatures: it is hence our "best" simulation.

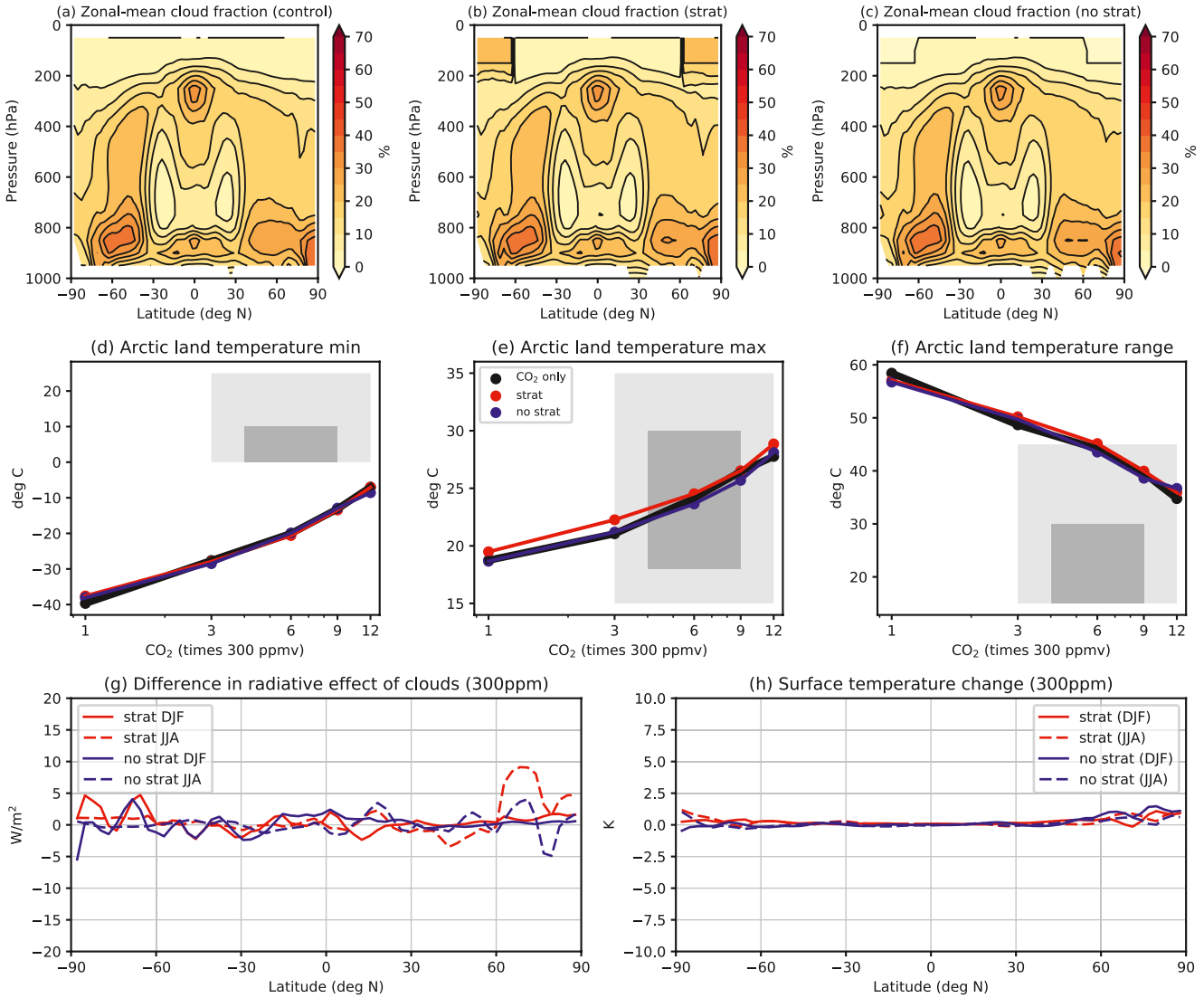

Figure 9. Prescribed Arctic stratospheric cloud experiments. Zonal-mean annual-mean cloud fraction for the control (a), increased stratospheric cloud (b), no stratospheric cloud (c) simulations at 300 ppm. Monthly minimum (d), maximum (e), and range (f) of Arctic land surface temperature for all three sets of simulations. The difference in radiative effect of clouds (g) and surface temperature change (h) between the prescribed cloud and control experiments at 300 ppm for Northern hemisphere winter (DJF) and summer (JJA). In panels (d, e, and f), the dark gray represents the values derived from Eberle et al. (2010), and the light gray is a larger interval to account for the uncertainty in proxy values.

6. Ocean Heat Transport

An increase in ocean heat transport has been sensibly posited to explain the reduced equator-to-pole temperature difference in the early Eocene climate. For example, Hotinski and Toggweiler (2003), using a diffusive atmospheric energy balance model, argued that an open Tethyan Passage could reduce the temperature difference between high and low latitudes by between 5°C and 9°C. However, other studies that use dynamical, three-dimensional atmospheric models have tended to find that changes in ocean heat transport are largely compensated by changes in atmospheric energy transport and the surface temperature is then largely unaltered, even over the ocean (Farneti & Vallis, 2013; Rencurrel & Rose, 2020).

We explore the importance of ocean heat transport by imposing a meridional heat flux (a "q-flux") to the slab ocean that mimics equator-to-pole energy transport by the ocean, as in Figure 11c. The flux is such as to give an ocean meridional energy flux of about 2.5 Petawatts in the Northern hemisphere in the 1x experiment (Figure 11d). (Note that since land masses are not taken into consideration in the ocean energy flux calculation, the integration

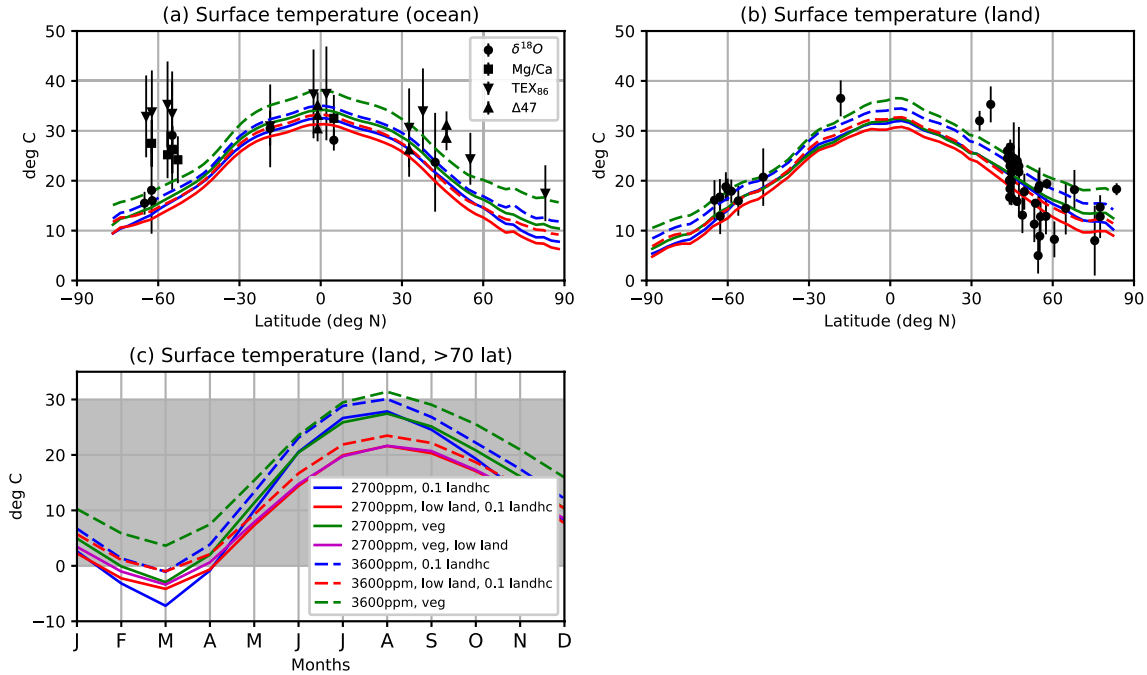

Figure 10. Increased land surface heat capacity experiments. Ocean (a) and land (b) annual-mean zonal-mean surface temperature. The root mean squared error between model and proxy values is 9.8, 10.8, 8.9, 8.3, 9.6, 7.4 K for ocean and 4.6, 5.3, 4.6, 4.9, 4.5, 5.8 K for land, for the "0.1 landhc" 2,700 ppm and 3,600 ppm simulations, the "low land, 0.1 landhc" 2,700 ppm and 3,600 ppm simulations, and the "veg" 2,700 ppm and 3,600 ppm simulations respectively. Seasonality of Arctic land temperature (c) for simulations with higher land surface heat capacity (blue), with higher land surface heat capacity and additional high-latitude low land clouds (red), with "modified vegetation" (increased land surface heat capacity, decreased albedo, and increased land evaporative resistance) (green), and with "modified vegetation" and additional high-latitude low land clouds (magenta) at 2,700 ppm (solid) and 3,600 ppm (dashed). In panels (a and b), the proxy values for ocean surface temperatures are compiled by Zhu et al. (2019) and the land surface temperatures are from Huber and Caballero (2011). In panel (c), the gray represents the values derived from Eberle et al. (2010).

of the q-flux does not exactly reach zero at the North pole (Figure 11d).) We then double the magnitude of the flux; these changes are considerably larger than the changes that might be expected in an Eocene climate. The imposed ocean heat transport cools the tropics and warms the subtropics very slightly where the q-flux is imposed (Figure 11a). However, perhaps surprisingly, enhanced ocean heat transport barely affects the Arctic land surface temperature (Figure 11b). This is not to say that the ocean heat flux has little effect; thus, for example, if the atmosphere is responding by changing its meridional energy flux then the intensity of its circulation (and hence such things as the mid-latitude storm tracks) will change correspondingly; however, we do not explore that here.

7. Conclusions and Discussion

In this paper we have explored the Eocene climate using a flexible climate model that allows us to explore in a controlled fashion the individual and combined effects of changes in cloudiness, surface properties, ocean heat transport, and CO_2 concentration. As well as comparing the simulation results to proxy estimates of the annual-mean zonal-mean surface temperature, we have explored the factors influencing the seasonality of high-latitude land surface temperature, with many of the proxy measurements taken from Eberle et al. (2010). Comparing the seasonality of the Eocene climate is quite a severe test of the verisimilitude of model simulations, since it is much harder to tune to observations simply by varying CO_2 levels than is annual mean temperature, and simultaneously tuning both annual mean temperature and seasonality is still more difficult.

The relative simplicity and flexibility of our climate model (compared, e.g., with "comprehensive" models used for global warming studies) allows us to explore the effects of changes in parameterizations or physical properties, recognizing both the incompleteness of the proxy data (compared to observations of today) and the uncertain accuracy of parameterizations in climate models especially when applied to a different climate. The radiation scheme used in our model (SOCRATES, Manners et al., 2017) is, however, quite accurate for CO_2 concentrations up to 32 times present day values. Our reference simulation—by which we mean simulations in which we change

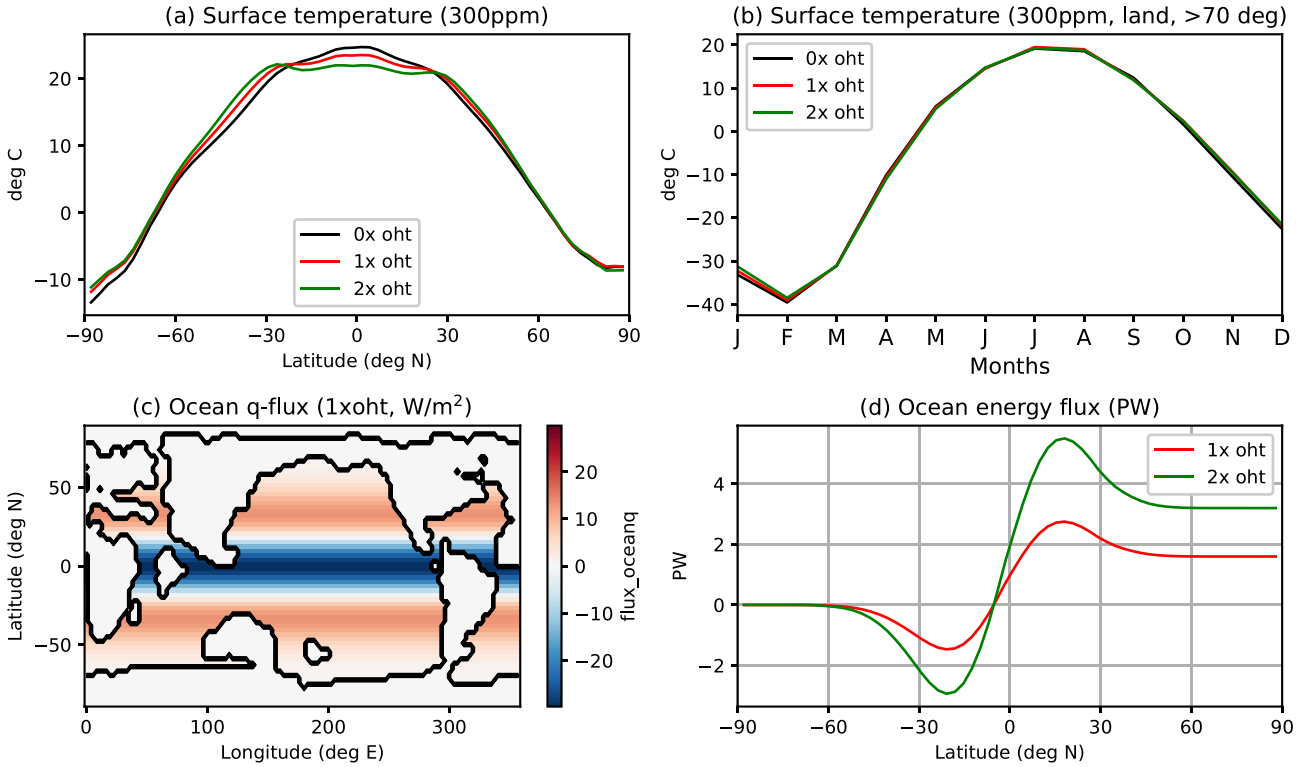

Figure 11. Ocean heat transport experiments. (a) Zonal-mean surface temperature and (b) land surface temperature poleward of 70 deg N for simulations with 0x, 1x, and 2x the ocean q-flux shown in (c), and corresponding ocean energy flux in (d). Note that since land masses are not taken into consideration in the ocean energy flux calculation, the integration of the q-flux does not reach 0 at the North pole.

only the CO_2 levels and leave other properties unaltered—at 12 × 300 ppm is actually reasonably close to values suggested by the proxies, certainly in the annual mean. A change in CO_2 levels is by far the most likely cause of increased Eocene temperatures. However, it is shown that a change in albedo has a similar gross effect (as noted by Carlson and Caballero (2017) and others). Such a change could occur due to changes in cloud distribution or in surface properties such as ice cover and vegetation, but the extent to which this can occur remains uncertain. In our simulations, the simulation with a 33% reduction in surface albedo (which can be considered a large reduction) has roughly the same temperature at 2,700 ppm as the reference 3,600 ppm simulation. An albedo change can thus help achieve an Eocene-like climate at lower CO_2 levels, but is not sufficient to be the dominant effect.

More difficulty arises in simulating the seasonal cycle, and in particular in obtaining winter temperatures that are more-or-less consistent with the proxies without going to CO_2 levels higher than proxies suggest and that would in turn lead to summer temperatures that are too high. Our simulations suggest that some changes in physical properties of the climate system (i.e., differences from the control simulation) are needed to achieve agreement. Having different cloud regimes is one plausible way, and one not necessarily well captured by GCMs. To test that, we explored the effects of *prescribing* various cloud distributions over land and/or ocean. Prescribing additional high clouds over the Arctic ocean, as might occur if there were enhanced convective activity in the warmer climate, has only a small impact on Arctic land temperatures in our simulations and is not a major factor in better satisfying the proxies. Similarly, increasing stratospheric clouds also has a relatively small effect. However, the presence of low clouds over land can have a larger effect, depending on the season and the CO_2 level. Prescribing additional low clouds over Arctic land increases winter Arctic land temperatures at low CO_2 levels, but has little effect at high CO_2 since the additional greenhouse effect is then relatively small. However, the increased low cloud does reduce summer Arctic land temperatures for all CO_2 levels, bringing Arctic land seasonality closer to the proxies.

The physical mechanisms whereby cloud cover might change in an Eocene climate are less clear. We found that the wetness of the land surface did have quite a large impact on low cloud formation over land, with increasing wetness leading to more low cloud. This is a plausibly important effect, given that the high-latitude land surface

in the Eocene may have been dotted with lakes and rainforest-like vegetation. Nevertheless, even with this effect, the only way to make the Arctic land above freezing year-round is to increase the land surface heat capacity over its present value by factor of 10. Although this may seem large the land heat capacity is still only 2 m equivalent water depth and is plausible given the difference in land-surface properties in the Eocene compared to those of today, where frozen land and ice cover give a very low heat capacity. If we additionally prescribe increased low land clouds that reduce summer Arctic land temperatures we come close to satisfying the proxies. Finally, we note that, perhaps surprisingly, even large changes in ocean heat transport have little impact on the zonal-mean surface temperature and none on Arctic land temperature seasonality (Figure 11). This is actually largely consistent with previous studies (Farneti & Vallis, 2013; Rencurrel & Rose, 2020).

While increased greenhouse gases seem to be a necessary condition to achieving an Eocene climate, it remains unclear if there is a unique combination of factors that is able to satisfy all available proxies, including the land surface temperature seasonality. There are, it seems, various pathways to get an Eocene climate simulation that is largely consistent with the various proxies.

1. By increasing CO_2 levels to 3,600 ppm the surface temperature is close to being within proxy bounds in the reference simulation (Figure 2). This level of CO_2 is higher than what is suggested by recent proxies (Anagnostou et al., 2020), which have a central estimate of around 2,000 ppm with an error bar extending to 3,000 ppm.
2. By reducing the surface albedo by about one third (as noted, a large reduction), the temperature is close to being within proxy bounds (Figure 4) at 2,700 ppm instead of 3,600 ppm.
3. Adding low clouds over high-latitude land reduces summer Arctic land temperatures for all CO_2 levels and increases winter Arctic land temperatures only at low CO_2 levels. Thus, at the higher levels of CO_2 appropriate for an Eocene climate, low clouds reduce the seasonality and help to bring the climate closer to the proxies (Figure 7).
4. Increasing the surface heat capacity of land has little effect on the meridional gradient in temperature, but reduces the Arctic land seasonality such that at 3,600 ppm, the land surface temperature is above freezing year-round (Figure 10) and only just below freezing in winter at 2,700 ppm.
5. Overall, the simulations "veg", "veg, low land" and "veg, low land, 0.1 landhc" (see Figure 10c) all match the proxies fairly well at 2,700 ppm, with land temperatures falling below freezing by at most 3°C in winter and staying well below the estimated maximum temperature in summer.

It may also be worth noting that our model has a somewhat low climate sensitivity (1.8 K for the reference climate compared to the current 2.3–4.5 K best estimate), which is probably due to the absence of sea ice and a relatively stabilizing cloud feedback. This may suggest that a higher sensitivity climate model (with less stabilizing cloud feedbacks) might better match the annual-average proxies for lower levels of CO_2, although since climate sensitivity increases at higher CO_2 levels such a direct comparison is difficult.

Given the relatively limited measurements, and the potentially similar effects that some of the changes have (e.g., reduced albedo vs. increased CO_2, increased low clouds and increased surface heat capacity), it is difficult to say what the "correct" set of parameters is that can reproduce an Eocene climate, although some scenarios are certainly more realistic than others. Undoubtedly, an increased level of CO_2 is needed, likely to values of above 1,800 ppm in order to reach the observed temperatures, even with the uncertainties present. A more precise value of required CO_2 levels cannot readily be estimated based on annual average considerations alone, but the seasonality provides a very useful additional constraint on model simulations. Our most plausible simulations arise with a CO_2 level of around 2,700 ppm with additional low cloud prescribed over land and a higher high-latitude heat capacity (Figure 10). These are all credible effects, given the likely change in surface properties (no sea ice, a wet, unfrozen land surface with increased vegetation and possible lakes) but we cannot be definitive. We also find that our reference 3,600 ppm simulation and the 2,700 ppm simulation with a 33% reduction in surface albedo are viable simulations of an Eocene climate, although such a reduction in surface albedo seems larger than could plausibly happen. Additional proxy measurements of seasonal information and surface properties, alongside more comprehensive simulations would further help reduce the uncertainty of both model parameterizations and the Eocene climate itself.

Finally, we draw some more general conclusions. The reduced equator-to-pole temperature gradient and much warmer winters over land of the early Eocene climate can, to a first approximation, be explained by robust, known

processes (specifically a combination of changes in lapse rates, Planck feedbacks, a higher surface heat capacity and possibly (and less well understood) cloud effects) and those effects can be captured by modern climate models, as both our results and those from the Deep-Time Model Intercomparison Project (DeepMIP) (Lunt et al., 2021) ensemble suggest. The proxies are not exactly matched by our simulations, but the differences are not large enough to suggest truly "unknown physics." For example, the Arctic land surface temperature our "modified vegetation" simulation at 9 × 300 ppm only falls below 0°C by 3°, and its annual-mean surface temperature is within the proxy uncertainty range of the majority of proxy data. Further, the reduced temperature gradient is likely not the result of a wholesale change in the general circulation of the atmosphere—the mid-troposphere temperature gradient need be little altered, for example. (We may note, though, that while unknown physics seem not to be necessary to explain the polar amplified temperature change and warmth over Arctic land in the high CO_2 early Eocene climate, the climates of periods such as the Oligocene and Miocene, which had lower CO_2 than the Eocene but still relatively high temperatures compared to today, seem to be not well captured by current climate models (Burls et al., 2021; Goldner et al., 2014; O'Brien et al., 2020) and the reasons for this are not fully understood.) Finally, care should be taken in using the Eocene to constrain the equilibrium climate sensitivity (to a doubling of CO_2 levels) of today's climate, for even if proxy temperature measurements were exact, effects not present in today's climate come into play. Purely radiative effects imply that the ECS will increase somewhat as temperature increases, and cloud and other feedbacks (both positive and negative) that are quantitatively different from those of today may arise in very warm climates, rendering extrapolation imprecise at best.

Data Availability Statement

The data is available at Henry and Vallis (2021a) and the code to reproduce the figures is available at Henry (2022). The proxy values for ocean surface temperature in Figures 2, 4, 5, and 10 are taken from Zhu et al. (2019). The proxy values for land surface temperature in Figures 2, 3, 4, 5, and 10 are taken from Huber and Caballero (2011).

Acknowledgments
We wish to thank all the Isca team for many discussions about climate and modeling, and in particular Stephen Thomson and Ruth Geen for help with the model setup and analysis. We also thank Eli Tziperman and Camille Hankel for a number of fruitful conversations about polar climates and clouds. This work was supported by NERC grant number NE/T00942X/1, under a NERC-NSF partnership named "Dynamics of Warm Past and Future Climates".

References

Abbot, D. S., & Tziperman, E. (2008). Sea ice, high-latitude convection, and equable climates. *Geophysical Research Letters*, *35*(3), L03702. https://doi.org/10.1029/2007gl032286

Anagnostou, E., John, E. H., Babila, T., Sexton, P., Ridgwell, A., Lunt, D. J., et al. (2020). Proxy evidence for state-dependence of climate sensitivity in the Eocene greenhouse. *Nature Communications*, *11*(1), 1–9. https://doi.org/10.1038/s41467-020-17887-x

Barrera, E. (1991). Paleogene and early Neogene oceanography of the southern Indian ocean: Leg 119 foraminifer stable isotope results. *Proceeding of the Ocean Drilling Program Science of Results*, *119*, 693–717.

Bijl, P. K., Bendle, J. A., Bohaty, S. M., Pross, J., Schouten, S., Tauxe, L., et al. (2013). Eocene cooling linked to early flow across the Tasmanian Gateway. *Proceedings of the National Academy of Sciences*, *110*(24), 9645–9650. https://doi.org/10.1073/pnas.1220872110

Bijl, P. K., Schouten, S., Sluijs, A., Reichart, G.-J., Zachos, J. C., & Brinkhuis, H. (2009). Early Palaeogene temperature evolution of the southwest Pacific Ocean. *Nature*, *461*(7265), 776–779. https://doi.org/10.1038/nature08399

Burke, K., Williams, J., Chandler, M., Haywood, A., Lunt, D., & Otto-Bliesner, B. (2018). Pliocene and Eocene provide best analogs for near-future climates. *Proceedings of the National Academy of Sciences*, *115*(52), 13288–13293. https://doi.org/10.1073/pnas.1809600115

Burls, N. J., Bradshaw, C., De Boer, A. M., Herold, N., Huber, M., Pound, M., et al. (2021). Simulating Miocene warmth: Insights from an opportunistic Multi-Model ensemble (MioMIP1). *Paleoceanography and Paleoclimatology*, *36*(5), e2020PA004054. https://doi.org/10.1029/2020pa004054

Caballero, R., & Huber, M. (2013). State-dependent climate sensitivity in past warm climates and its implications for future climate projections. *Proceedings of the National Academy of Sciences*, *110*(35), 14162–14167. https://doi.org/10.1073/pnas.1303365110

Carlson, H., & Caballero, R. (2017). Atmospheric circulation and hydroclimate impacts of alternative warming scenarios for the Eocene. *Climate of the Past*, *13*(8), 1037–1048. https://doi.org/10.5194/cp-13-1037-2017

Cramwinckel, M. J., Huber, M., Kocken, I. J., Agnini, C., Bijl, P. K., Bohaty, S. M., et al. (2018). Synchronous tropical and polar temperature evolution in the Eocene. *Nature*, *559*(7714), 382–386. https://doi.org/10.1038/s41586-018-0272-2

Creech, J. B., Baker, J. A., Hollis, C. J., Morgans, H. E., & Smith, E. G. (2010). Eocene sea temperatures for the mid-latitude southwest pacific from mg/ca ratios in planktonic and benthic foraminifera. *Earth and Planetary Science Letters*, *299*(3–4), 483–495. https://doi.org/10.1016/j.epsl.2010.09.039

Cronin, T. W., & Jansen, M. F. (2016). Analytic radiative-advective equilibrium as a model for high-latitude climate. *Geophysical Research Letters*, *43*(1), 449–457. https://doi.org/10.1002/2015gl067172

Cronin, T. W., Li, H., & Tziperman, E. (2017). Suppression of Arctic air formation with climate warming: Investigation with a two-dimensional cloud-resolving model. *Journal of the Atmospheric Sciences*, *74*(9), 2717–2736. https://doi.org/10.1175/jas-d-16-0193.1

Cronin, T. W., & Tziperman, E. (2015). Low clouds suppress Arctic air formation and amplify high-latitude continental winter warming. *Proceedings of the National Academy of Sciences*, *112*(37), 11490–11495. https://doi.org/10.1073/pnas.1510937112

Eberle, J. J., Fricke, H. C., Humphrey, J. D., Hackett, L., Newbrey, M. G., & Hutchison, J. H. (2010). Seasonal variability in arctic temperatures during early Eocene time. *Earth and Planetary Science Letters*, *296*(3–4), 481–486. https://doi.org/10.1016/j.epsl.2010.06.005

Evans, D., Sagoo, N., Renema, W., Cotton, L. J., Müller, W., Todd, J. A., et al. (2018). Eocene greenhouse climate revealed by coupled clumped isotope-mg/ca thermometry. *Proceedings of the National Academy of Sciences*, *115*(6), 1174–1179. https://doi.org/10.1073/pnas.1714744115

Farneti, R., & Vallis, G. K. (2013). Meridional energy transport in the coupled atmosphere–ocean system: Compensation and partitioning. *Journal of Climate*, *26*(18), 7151–7166. https://doi.org/10.1175/jcli-d-12-00133.1

Feldl, N., Po-Chedley, S., Singh, H. K., Hay, S., & Kushner, P. J. (2020). Sea ice and atmospheric circulation shape the high-latitude lapse rate feedback. *NPJ Climate and Atmospheric Science*, *3*(1), 1–9. https://doi.org/10.1038/s41612-020-00146-7

Frieling, J., Iakovleva, A. I., Reichart, G.-J., Aleksandrova, G. N., Gnibidenko, Z. N., Schouten, S., & Sluijs, A. (2014). Paleocene–Eocene warming and biotic response in the epicontinental West Siberian Sea. *Geology*, *42*(9), 767–770. https://doi.org/10.1130/g35724.1

Frierson, D. M. (2007). The dynamics of idealized convection schemes and their effect on the zonally averaged tropical circulation. *Journal of the Atmospheric Sciences*, *64*(6), 1959–1976. https://doi.org/10.1175/jas3935.1

Goldner, A., Herold, N., & Huber, M. (2014). The challenge of simulating the warmth of the mid-Miocene climatic optimum in CESM1. *Climate of the Past*, *10*(2), 523–536. https://doi.org/10.5194/cp-10-523-2014

Graversen, R. G., & Wang, M. (2009). Polar amplification in a coupled climate model with locked albedo. *Climate Dynamics*, *33*(5), 629–643. https://doi.org/10.1007/s00382-009-0535-6

Greenwood, D. R., & Wing, S. L. (1995). Eocene continental climates and latitudinal temperature gradients. *Geology*, *23*(11), 1044–1048. https://doi.org/10.1130/0091-7613(1995)023<1044:eccalt>2.3.co;2

Henry, M. (2022). matthewjhenry/eocene: Code for figures in "Variations on a Pathway to an Early Eocene Climate." by Henry and Vallis (2022). (v.1.0.1). Zenodo, [Software]. https://doi.org/10.5281/zenodo.6980289

Henry, M., Merlis, T. M., Lutsko, N. J., & Rose, B. E. (2021). Decomposing the drivers of polar amplification with a single-column model. *Journal of Climate*, *34*(6), 2355–2365. https://doi.org/10.1175/jcli-d-20-0178.1

Henry, M., & Vallis, G. K. (2021a). Idealized GCM dataset for "Different Pathways to an Early Eocene Climate" by Matthew Henry and Geoffrey K. Vallis. Zenodo. [Dataset]. https://doi.org/10.5281/zenodo.5591825

Henry, M., & Vallis, G. K. (2021b). Reduced high-latitude land seasonality in climates with very high carbon dioxide. *Journal of Climate*, 1–38. https://doi.org/10.1175/jcli-d-21-0131.1

Herold, N., Buzan, J., Seton, M., Goldner, A., Green, J., Müller, R., et al. (2014). A suite of early Eocene (˜55 ma) climate model boundary conditions. *Geoscientific Model Development*, *7*(5), 2077–2090. https://doi.org/10.5194/gmd-7-2077-2014

Hines, B. R., Hollis, C. J., Atkins, C. B., Baker, J. A., Morgans, H. E., & Strong, P. C. (2017). Reduction of oceanic temperature gradients in the early Eocene southwest pacific ocean. *Palaeogeography, Palaeoclimatology, Palaeoecology*, *475*, 41–54. https://doi.org/10.1016/j.palaeo.2017.02.037

Holland, M. M., & Bitz, C. M. (2003). Polar amplification of climate change in coupled models. *Climate Dynamics*, *21*(3), 221–232. https://doi.org/10.1007/s00382-003-0332-6

Hollis, C. J., Dunkley Jones, T., Anagnostou, E., Bijl, P. K., Cramwinckel, M. J., Cui, Y., et al. (2019). The DeepMIP contribution to PMIP4: Methodologies for selection, compilation and analysis of latest Paleocene and early Eocene climate proxy data, incorporating version 0.1 of the DeepMIP database. *Geoscientific Model Development*, *12*(7), 3149–3206. https://doi.org/10.5194/gmd-12-3149-2019

Hollis, C. J., Handley, L., Crouch, E. M., Morgans, H. E., Baker, J. A., Creech, J., et al. (2009). Tropical sea temperatures in the high-latitude south pacific during the Eocene. *Geology*, *37*(2), 99–102. https://doi.org/10.1130/g25200a.1

Hollis, C. J., Hines, B., Littler, K., Villasante-Marcos, V., Kulhanek, D., Strong, C., et al. (2015). The Paleocene–Eocene thermal maximum at DSDP site 277, Campbell plateau, southern pacific ocean. *Climate of the Past*, *11*(7), 1009–1025. https://doi.org/10.5194/cp-11-1009-2015

Hollis, C. J., Taylor, K. W., Handley, L., Pancost, R. D., Huber, M., Creech, J. B., et al. (2012). Early Paleogene temperature history of the Southwest Pacific Ocean: Reconciling proxies and models. *Earth and Planetary Science Letters*, *349*, 53–66. https://doi.org/10.1016/j.epsl.2012.06.024

Hotinski, R., & Toggweiler, J. (2003). Impact of a Tethyan circumglobal passage on ocean heat transport and "equable" climates. *Paleoceanography*, *18*(1). https://doi.org/10.1029/2001pa000730

Hu, Z., Cronin, T. W., & Tziperman, E. (2018). Suppression of Cold Weather Events over High-Latitude Continents in Warm Climates. *Journal of Climate*, *31*(23), 9625–9640. https://doi.org/10.1175/jcli-d-18-0129.1

Huber, M., & Caballero, R. (2011). The early Eocene equable climate problem revisited. *Climate of the Past*, *7*(2), 603–633. https://doi.org/10.5194/cp-7-603-2011

Huber, M., Sloan, L. C., & Shellito, C. (2003). Early Paleogene oceans and climate: A fully coupled modeling approach using the NCAR CCSM. *Geological Society of America Special Paper*, *369*, 25–47.

Inglis, G. N., Farnsworth, A., Lunt, D., Foster, G. L., Hollis, C. J., Pagani, M., et al. (2015). Descent toward the icehouse: Eocene sea surface cooling inferred from GDGT distributions. *Paleoceanography*, *30*(7), 1000–1020. https://doi.org/10.1002/2014pa002723

John, C. M., Bohaty, S. M., Zachos, J. C., Sluijs, A., Gibbs, S., Brinkhuis, H., & Bralower, T. J. (2008). North American continental margin records of the Paleocene-Eocene thermal maximum: Implications for global carbon and hydrological cycling. *Paleoceanography*, *23*(2). https://doi.org/10.1029/2007pa001465

Jucker, M., & Gerber, E. (2017). Untangling the annual cycle of the tropical tropopause layer with an idealized moist model. *Journal of Climate*, *30*(18), 7339–7358. https://doi.org/10.1175/jcli-d-17-0127.1

Keating-Bitonti, C. R., Ivany, L. C., Affek, H. P., Douglas, P., & Samson, S. D. (2011). Warm, not super-hot, temperatures in the early Eocene subtropics. *Geology*, *39*(8), 771–774. https://doi.org/10.1130/g32054.1

Kiehl, J. T., & Shields, C. A. (2013). Sensitivity of the Palaeocene–Eocene Thermal Maximum climate to cloud properties. *Philosophical Transactions of the Royal Society A: Mathematical, Physical & Engineering Sciences*, *371*(2001), 20130093. https://doi.org/10.1098/rsta.2013.0093

Kozdon, R., Kelly, D. C., Kita, N. T., Fournelle, J. H., & Valley, J. W. (2011). Planktonic foraminiferal oxygen isotope analysis by ion microprobe technique suggests warm tropical sea surface temperatures during the early Paleogene. *Paleoceanography*, *26*(3). https://doi.org/10.1029/2010pa002056

Liu, Q., Collins, M., Maher, P., Thomson, S. I., & Vallis, G. K. (2020). Simcloud version 1.0: A simple diagnostic cloud scheme for idealized climate models. *Geoscientific Model Development Discussions*, *14*(5), 1–39. https://doi.org/10.5194/gmd-14-2801-2021

Lu, G., & Keller, G. (1993). The Paleocene-Eocene transition in the Antarctic Indian Ocean: Inference from planktic foraminifera. *Marine Micropaleontology*, *21*(1–3), 101–142. https://doi.org/10.1016/0377-8398(93)90012-m

Lunt, D. J., Bragg, F., Chan, W.-L., Hutchinson, D. K., Ladant, J.-B., Morozova, P., et al. (2021). DeepMIP: Model intercomparison of early Eocene climatic optimum (EECO) large-scale climate features and comparison with proxy data. *Climate of the Past*, *17*(1), 203–227. https://doi.org/10.5194/cp-17-203-2021

Manners, J., Edwards, J. M., Hill, P., & Thelen, J.-C. (2017). *SOCRATES: Suite of Community RAdiative Transfer codes based on Edwards and Slingo (Tech. Rep.)*. UK Met Office.

Merlis, T. M., Schneider, T., Bordoni, S., & Eisenman, I. (2013). Hadley circulation response to orbital precession. Part ii: Subtropical continent. *Journal of Climate*, *26*(3), 754–771. https://doi.org/10.1175/jcli-d-12-00149.1

O'Brien, C. L., Huber, M., Thomas, E., Pagani, M., Super, J. R., Elder, L. E., & Hull, P. M. (2020). The enigma of Oligocene climate and global surface temperature evolution. *Proceedings of the National Academy of Sciences*, *117*(41), 25302–25309. https://doi.org/10.1073/pnas.2003914117

Pearson, P. N., van Dongen, B. E., Nicholas, C. J., Pancost, R. D., Schouten, S., Singano, J. M., & Wade, B. S. (2007). Stable warm tropical climate through the Eocene epoch. *Geology*, *35*(3), 211–214. https://doi.org/10.1130/g23175a.1

Pierrehumbert, R. T. (2010). *Principles of planetary climate*. Cambridge University Press.

Rae, J. W., Zhang, Y. G., Liu, X., Foster, G. L., Stoll, H. M., & Whiteford, R. D. (2021). Atmospheric CO_2 over the past 66 million years from marine archives. *Annual Review of Earth and Planetary Sciences*, *49*(1), 609–641. https://doi.org/10.1146/annurev-earth-082420-063026

Rencurrel, M. C., & Rose, B. E. (2020). The efficiency of the Hadley cell response to wide variations in ocean heat transport. *Journal of Climate*, *33*(5), 1643–1658. https://doi.org/10.1175/jcli-d-19-0334.1

Sherwood, S., Webb, M. J., Annan, J. D., Armour, K., Forster, P. M., Hargreaves, J. C., et al. (2020). An assessment of Earth's climate sensitivity using multiple lines of evidence. *Reviews of Geophysics*, *58*(4), e2019RG000678. https://doi.org/10.1029/2019rg000678

Sloan, L. C., & Pollard, D. (1998). Polar stratospheric clouds: A high latitude warming mechanism in an ancient greenhouse world. *Geophysical Research Letters*, *25*(18), 3517–3520. https://doi.org/10.1029/98gl02492

Sluijs, A., Schouten, S., Pagani, M., Woltering, M., Brinkhuis, H., Damsté, J. S. S., et al. (2006). Subtropical Arctic Ocean temperatures during the Palaeocene/Eocene thermal maximum. *Nature*, *441*(7093), 610–613. https://doi.org/10.1038/nature04668

Stott, L. D., Kennett, J. P., Shackleton, N. J., & Corfield, R. M. (1990). 48. the evolution of Antarctic surface waters during the PALEOGENE: Inferences from the stable isotopic composition of planktonic foraminifers, ODP leg 1131. *Proceeding of the Ocean Drilling Program Science of Results*, *113*, 849–863.

Swann, A. L., Fung, I. Y., Levis, S., Bonan, G. B., & Doney, S. C. (2010). Changes in arctic vegetation amplify high-latitude warming through the greenhouse effect. *Proceedings of the National Academy of Sciences*, *107*(4), 1295–1300. https://doi.org/10.1073/pnas.0913846107

Taylor, P. C., Boeke, R. C., Boisvert, L. N., Feldl, N., Henry, M., Langen, P. L., et al. (2021). Process drivers, inter-model spread, and the path forward: A review of amplified arctic warming. *EarthArxiv Preprint*. https://doi.org/10.31223/X5VS6C

Thomson, S. I., & Vallis, G. K. (2019). The effects of gravity on the climate and circulation of a terrestrial planet. *Quarterly Journal of the Royal Meteorological Society*, *145*(723), 2627–2640. https://doi.org/10.1002/qj.3582

Tierney, J. E., Poulsen, C. J., Montañez, I. P., Bhattacharya, T., Feng, R., Ford, H. L., et al. (2020). Past climates inform our future. *Science*, *370*(6517). https://doi.org/10.1126/science.aay3701

Tripati, A. K., Delaney, M. L., Zachos, J. C., Anderson, L. D., Kelly, D. C., & Elderfield, H. (2003). Tropical sea-surface temperature reconstruction for the early Paleogene using mg/ca ratios of planktonic foraminifera. *Paleoceanography*, *18*(4). https://doi.org/10.1029/2003pa000937

Vallis, G. K., Colyer, G., Geen, R., Gerber, E., Jucker, M., Maher, P., et al. (2018). Isca, v1. 0: A framework for the global modelling of the atmospheres of earth and other planets at varying levels of complexity. *Geoscientific Model Development*, *11*(3), 843–859. https://doi.org/10.5194/gmd-11-843-2018

Zhu, J., Poulsen, C. J., & Tierney, J. E. (2019). Simulation of Eocene extreme warmth and high climate sensitivity through cloud feedbacks. *Science Advances*, *5*(9), eaax1874. https://doi.org/10.1126/sciadv.aax1874